Three-scale model of single bone osteon modelled as double-porous fluid saturated body: Study of influence of micro/meso-structure

J. Turjanicová[a,*], E. Rohan[a], S. Naili[b]

[a]*Faculty of Applied Sciences, University of West Bohemia, Univerzitní 22, 306 14 Plzeň, Czech Republic*

[b]*Laboratoir modelisation et simulation multi échelle, Université Paris-est, 61 avenue du Général de Gaulle, Créteil cedex, France*

Abstract

This paper deals with the multiscale description of a single osteon of cortical bones. The cortical bone tissue is modeled as a double-porous medium decomposed into the solid matrix and the fluid saturated canals. The resulting homogenized model describes deformation of such medium in response to a static loading by external forces and to an injection of slightly compressible fluid. Three numerical examples are presented, showing the influence of selected lower-scales geometrical features on the macroscopic body behavior.
© 2014 University of West Bohemia. All rights reserved.

Keywords: homogenization, poroelasticity, osteon, cortical bone

1. Introduction

This paper is devoted to the macroscopic behavior of the poroelastic materials with the double porosity. Such materials consist of two very distinct porous systems so that their interaction has a strong influence on their macroscopic behavior. The two interacting systems featured by strongly different pore sizes are arranged hierarchically, one is embedded in the other. This characterizes materials which are abundant in nature, such as rocks, or biological tissues, as well as engineered materials comprising certain types of foams. The model reported in this paper can be applied to describe the cortical bone tissue, where the pores filled with bone fluid can be found on multiple scales. The material properties of the bone can serve as a basis for the development of new biomaterials or for a better understanding of the processes in the bone tissue such as remodeling.

The concept of double porosity was first presented in context of geomechanics in work [1], which studied flows in cracked rocks. This work considered only the fluid exchange between two porous systems. The model was simplified few years later in work [10], where authors considered situation such that the flow in the porous matrix can be neglected. Under the same assumption, in the recent work [6] we presented a model of the double-porous medium derived using unfolding homogenization method applied at two levels of the heterogeneity coressponding to a hierarchical arrangement of the bone sructure. This model can be used to compute the effective poroelasticity coefficients for a given geometry and topology of the micro- and mesoscopic levels.

The aim of this paper is to perform a computational study which explains how the micro- and mesostructure influence the macroscopic body response. We focus on the poroelastic properties

---

*Corresponding author. Tel.: +420 377 632 387, e-mail: turjani@kme.zcu.cz.

which are independent of the pore fluid flow. The solid-fluid interaction is studied under the static loading whereby any fluid flow is excluded. It should be emphasized that the poroelastic material constants derived and computed under such thermodynamic steady state conditions are valid also in quasistatic situations featured by slow flows; this has been justified, e.g., in [3, 8].

The paper is composed from five sections. In the Section 2 the definition and the geometry description of porosity levels is given. The following Section 3 deals with the upscaling procedure of equations describing poroelasticity. The Section 4 introduces the set of numerical simulations with their results discussed. Finally, a conclusion is drawn in Section 5.

2. Geometrical configuration

The cortical bone is a hierarchical system with a complex structure on different scale levels. From the macroscopic point of view, the cortical bone tissue is made of a system of approximately cylindrical mineralized structures called osteons, each with an exterior radius of roughly 100–$150\,\mu$m, [11]. These structures are hollow; the center of each osteon is perforated by the so-called Haversian canal, which contains blood vessels, nerves, and is saturated by the bone fluid. In addition to these canals, other smaller pathways exist within the bone tissue. The aim of this section is to describe this multiscale arrangement of the bone tissue and, in particular, to explain geometry of the structure.

The walls of the Haversian canal are covered with bone cells and behind this bone cell layer, there are entrances to multiple small tunnels [11]. These tunnels with the diameters of a few hundreds of nanometers are called canaliculi and create the network connecting Haversian canal and the small ellipsoidal pores. These are called lacunae with dimension about a few tens of micrometers and each of them contains one osteocyte, the bone cell responsible for the tissue growth processes. Canaliculi and lacunae create one system of a mutually connected network filled with bone fluid.

In literature, [2, 4, 11], there are commonly distinguished three porosity levels with the biggest importance in the bone structure. The uppermost level is the so-called vascular porosity level involving the Haversian canals, the mean one, the lacunar-canalicular porosity, is associated with lacunae and canaliculi, and lowest one is the collagen-apatite porosity associated with the space between collagen and the crystallites of the mineral apatite.

The present work is focused on describing the mechanical properties of the single bone osteon which is relevant to the macroscopic scale. Therefore, we shall neglect the vascular porosity (or osteonal porosity). Considering the difference in dimensions of lacunae and canaliculi, the lacuno-canalicular porosity is split into two levels; the lacunar porosity further referred to as a mesoscopic porosity level or β-level and canalicular porosity referred to as microscopic porosity or α-level. Porosity of the collagen-apatite matrix is neglected in this work, being replaced by a solid elastic material.

In the numerical examples reported in Section 4 we shall represent the hierarchical structure of the osteon using a simple geometrical models which, however, enable us to introduce geometrical parameters with a clear interpretation and to assess their influence on the effective material properties.

3. Homogenized model

In this section we summarize the homogenization results witch was obtained in [6] by unfolding homogenization method of the poroelasticity problem in a dual porous medium saturated by a slightly compressible fluid. In throughout the text, we use labelling by two superscripts: α for microscopic (or α-) level and β for mesoscopic (β-) level. First, we recall a few general

Table 1. Basic nomenclature

Superscript	Describtion	Superscript	Describtion
$\square^{\varepsilon}$	quantities dependent on the scale-parameter	$\square^{m}$	quantities defined on matrix (solid)
$\square^{\alpha}$	quantities relevant to the microscopic level	$\square^{c}$	quantities defined on canals (fluid)
$\square^{\beta}$	quantities relevant to the mesoscopic level		
Quantity	Describtion	Quantity	Describtion
$\mathbf{u}$	displacement	$\mathbf{v}$	admissible displacement
$\tilde{\mathbf{u}}$	matrix-to-canal extension of $\mathbf{u}$	$\bar{p}$	fluid pressure
$\mathbf{f}$	volume forces	$\mathbf{g}$	traction forces
γ	fluid compressibility	J	fluid volume (injected)
ω^{ij}	characteristic responses relevant to displacement	ϕ	porosity
ω^{P}	characteristic responses relevant to pressure	$\mathbb{D} = (D_{ijkl})$	elasticity tensor
$\mathbf{\Pi}^{ij} = (\Pi_k^{ij})$	transformation vectors, $k = 1, 2, 3$	$\mathbf{n}$	outer unit normal vector
$\mathbb{A} = (A_{ijkl})$	effective elasticity tensor	$\mathbf{B} = (B_{ij})$	effective tensor of Biot coefficients
M	effective Biot modulus of compressibility	E	Young's modulus
G	shear modulus	ν	Poisson's ratio

principles of homogenization and then we focus on the microscopic scale problem. It is worth noting, that for the better orientation throught text, the used notation is summarized in Table 1.

3.1. Scale parameter

We consider a poroelastic medium whose material properties vary periodically with position; the period length is proportional to a small parameter ε which is the so called scale-parameter defined as the ratio between the characteristic lengths of the micro- and macroscopic levels, thus, $\varepsilon = L_{micro}/L_{macro}$.

Through the text all quantities varying with this periodicity are denoted with superscript $^{\varepsilon}$. In our case we have three scales, micro-, meso- and macro-scale, thus it is more accurate to define scale-parameter as ratio of characteristic length of lower and upper scale.

3.2. Material periodicity

For simplicity we consider material with the periodic geometrical decomposition on both the micro- and mesoscale. The following general definition applies to both α and β levels and through the text all quantities belonging to those levels are labelled by superscripts $^{\alpha}$ and $^{\beta}$.

We consider an open bounded domain $\Omega \in \mathbb{R}^3$ with boundary $\partial\Omega$. Further we consider domain $Y = \prod_{i=1}^3 (0, \hat{y}_i)$ which is called the representative periodic cell (RPC), since it generates the domain Ω as a periodic lattice. The material point positions are defined in the coordinate system $(0, x_1, x_2, x_3)$. The rescaled material point positions in the RPC are defined in the coordinate system $(\hat{0}, y_1, y_2, y_3)$, where $\hat{y}_i$ is the length of the i-th side of Y.

Application of this definition to the three scale model is illustrated in the Fig. 1. Thus, the domain Ω is generated (as periodic lattice) by using mesoscopic RPC Y^{β}. The matrix part
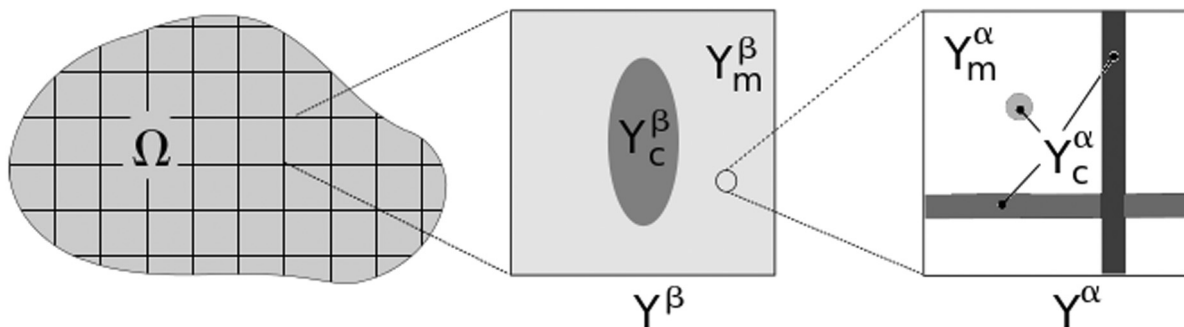

Fig. 1. Three scales of homogenization: Macroscopic body Ω, mesoscopic periodic cell Y^{β}, microscopic cell Y^{α}

within Y^β is also generated as periodic structure by using a microscopic RPC Y^α. Details are given below.

3.3. Microscopic problem

Let us consider $\Omega^\alpha \subset \mathbf{R}^3$, which represents the microscopic scale of the osteon. With respect to the material structure, the domain $\Omega^\alpha \subset \mathbf{R}^3$ is decomposed into two non-overlapping parts; the (solid) matrix $\Omega_m^{\alpha,\varepsilon}$, canals $\Omega_c^{\alpha,\varepsilon}$ and their interface $\Gamma^{\alpha,\varepsilon}$ are defined, as follows:

$$\Omega^\alpha = \Omega_m^{\alpha,\varepsilon} \cup \Omega_c^{\alpha,\varepsilon} \cup \Gamma^{\alpha,\varepsilon}, \qquad \Omega_c^{\alpha,\varepsilon} = \Omega^{\alpha,\varepsilon} \setminus \bar\Omega_m^{\alpha,\varepsilon}, \quad \Gamma^{\alpha,\varepsilon} = \bar\Omega_m^{\alpha,\varepsilon} \cap \bar\Omega_c^{\alpha,\varepsilon} . \tag{1}$$

The outer boundaries $\partial_{ext}\Omega_c^{\alpha,\varepsilon} \subset \partial\Omega^\alpha$ and $\partial_{ext}\Omega_m^{\alpha,\varepsilon} \subset \partial\Omega^\alpha$, are defined as follows:

$$\partial_{ext}\Omega_m^{\alpha,\varepsilon} = \partial\Omega_m^{\alpha,\varepsilon} \setminus \Gamma^{\alpha,\varepsilon} = \partial\Omega_m^{\alpha,\varepsilon} \cap \partial\Omega^\alpha, \qquad \partial_{ext}\Omega_c^{\alpha,\varepsilon} = \partial\Omega_c^{\alpha,\varepsilon} \setminus \Gamma^{\alpha,\varepsilon} = \partial\Omega_c^{\alpha,\varepsilon} \cap \partial\Omega^\alpha. \tag{2}$$

The outer unit normal vectors of the boundaries $\partial\Omega_m^{\alpha,\varepsilon}$ and $\partial\Omega_c^{\alpha,\varepsilon}$ are denoted by $\mathbf{n}^m$ and $\mathbf{n}^c$, respectively. In this section, the superscript $^\varepsilon$ refers to the scale-dependence, where $\varepsilon = L_\alpha/L_\beta$ describes the ration of the characteristic sizes of the micro- and mesoscopic levels.

In what follows, we will use the same notation as in [6]. By symbols ∇ and $\nabla\cdot$ the gradient and divergence operators are denoted, respectively. The scalar product is denoted by "·" and the symbol ":" between tensors of any order denotes their double contraction. The superscript s in the gradient operator ∇^s denotes its symmetric part.

The linear poroelastic body characterized by its elasticity tensor D_{ijkl}^ε, occupying the domain $\Omega^\alpha \subset \mathbf{R}^3$, is loaded by volume forces $\mathbf{f}^{\alpha,\varepsilon}$ in $\Omega_m^{\alpha,\varepsilon}$ and surface traction forces $\mathbf{g}^{\alpha,\varepsilon}$ on $\partial_{ext}\Omega_m^{\alpha,\varepsilon}$.

Since the objective here is to characterize the effective poroelastic properties of the bone tissue, we restrict ourselves to the stationary problems only and neglect the fluid flow. Therefore, the fluid in the deforming pores is characterized by its compressibility γ only, whereas its viscosity does not interfere in the problem. Further, mass conservation has to be considered: The pore deformation resulting in a decrease of the porosity is compensated by an increased pressure acting on the interface Γ_{mc} and by an amount of the fluid leaking from $\Omega_c^{\alpha,\varepsilon}$ into the outer space through $\partial_{ext}\Omega_c^{\alpha,\varepsilon}$, cf. [6]. Using the tensorial notation, the linear poroelasticity problem is defined as follows

$$\begin{aligned}
-\nabla(\mathbb{D}^{\alpha,\varepsilon}\nabla^S\mathbf{u}^{\alpha,\varepsilon}) &= \mathbf{f}^{\alpha,\varepsilon} & \text{in} & \quad \Omega_m^{\alpha,\varepsilon}, \\
\mathbf{n}^m \cdot \mathbb{D}^{\alpha,\varepsilon}\nabla^S\mathbf{u}^{\alpha,\varepsilon} &= \mathbf{g}^{\alpha,\varepsilon} & \text{on} & \quad \partial_{ext}\Omega_m^{\alpha,\varepsilon}, \\
\mathbf{n}^m \cdot \mathbb{D}^{\alpha,\varepsilon}\nabla^S\mathbf{u}^{\alpha,\varepsilon} &= -\bar{p}^{\alpha,\varepsilon} & \text{on} & \quad \Gamma^{\alpha,\varepsilon},
\end{aligned} \tag{3}$$

where $\mathbf{u}^{\alpha,\varepsilon}$ is the displacement of the solid matrix and $\bar{p}^{\alpha,\varepsilon}$ is the fluid pressure. The announced mass conservation attains the following form

$$\int_{\partial\Omega_c^{\alpha,\varepsilon}} \tilde{\mathbf{u}}^{\alpha,\varepsilon} \cdot \mathbf{n}^c \, \mathrm{d}S_x + \gamma\bar{p}^{\alpha,\varepsilon}|\Omega_c^{\alpha,\varepsilon}| = -J^{\alpha,\varepsilon}, \tag{4}$$

where $-J^{\alpha,\varepsilon}$ denotes a fluid volume injected from outside through $\partial_{ext}\Omega_c^{\alpha,\varepsilon}$ into $\Omega_c^{\alpha,\varepsilon}$. By $\tilde{\mathbf{u}}$ we mean a matrix-to-canal differentiable extension of $\mathbf{u}$ from Ω_m^ε to whole Ω.

The solvability condition yields $\int_{\partial_{ext}\Omega_m^{\alpha,\varepsilon}} \mathbf{g}^{\alpha,\varepsilon} \, \mathrm{d}S_x + \int_{\Omega_m^{\alpha,\varepsilon}} \mathbf{f}^{\alpha,\varepsilon} \, \mathrm{d}V_x = \mathbf{0}$, where $\mathrm{d}S_x$ is the differential element of the surface and $\mathrm{d}V_x$ of the volume.

Weak formulation   We introduce set of admissible displacements V, which due to assumed boundary conditions $(3)_{2,3}$ coincide with the space of virtual displacement $V = V_0 = \{\mathbf{v} \in \mathbf{H}^1(\Omega_m^{\alpha,\varepsilon}) | \mathbf{v} = \overline{\mathbf{u}} \text{ on } \partial_{ext}\Omega_m^{\alpha,\varepsilon}\}$, where $\mathbf{H}^1$ is the Sobolev space $[W^{1,2}(\Omega^\alpha)]^3$ of vector functions. The problem (3)–(4) can be rewritten in the weak form[1]: Find $(\boldsymbol{u}^{\alpha,\varepsilon}, \bar{p}^{\alpha,\varepsilon}) \in \mathbf{H}^1(\Omega_m^{\alpha,\varepsilon}) \times \mathbb{R}$ such that

$$\int_{\Omega_m^{\alpha,\varepsilon}} (\mathbf{D}^{\alpha,\varepsilon}\nabla^s\mathbf{u}^{\alpha,\varepsilon}) : \nabla^s\mathbf{v} \; \mathrm{dV}_x + \bar{p}^{\alpha,\varepsilon} \int_{\Gamma_m^{\alpha,\varepsilon}} \mathbf{n}^m \cdot \mathbf{v} \; \mathrm{dS}_x = \int_{\partial_{ext}\Omega_m^{\alpha,\varepsilon}} \mathbf{g}^{\alpha,\varepsilon} \cdot \mathbf{v} \; \mathrm{dS}_x + \int \mathbf{f}^{\alpha,\varepsilon} \cdot \mathbf{v} \; \mathrm{dV}_x,$$

$$\int_{\partial\Omega_c^{\alpha,\varepsilon}} \tilde{\mathbf{u}}^{\alpha,\varepsilon} \cdot \mathbf{n}^c \; \mathrm{d}S_x + \gamma\bar{p}^{\alpha,\varepsilon}|\Omega_c^{\alpha,\varepsilon}| = -J^{\alpha,\varepsilon} \qquad \forall\mathbf{v} \in V_0.$$

(5)

3.3.1.   Representative periodic cell (RPC)

The domain Ω^α representing the periodic microstructure is generated by representative cell Y^α which adheres the decomposition introduced in (1), thus,

$$Y^\alpha = Y_m^\alpha \cup Y_c^\alpha \cup \Gamma_{mc}, \qquad Y_c^\alpha = Y^\alpha \setminus \bar{Y}_m^\alpha, \qquad \Gamma_{mc} = \bar{Y}_m^\alpha \cap \bar{Y}_c^\alpha. \tag{6}$$

We assume that the elastic tensor parameters $D_{ijkl}^{\alpha,\varepsilon}$ obey the standard positive definiteness and symmetries; in our study we consider an isotropic material[2] $D_{ijkl}^{\alpha,\varepsilon}(x) = \lambda^\varepsilon(x)\delta_{kl}\delta_{ij} + \mu^\varepsilon(x)(\delta_{ik}\delta_{jl} + \delta_{il}\delta_{jk})$ with the Lame coefficients $\lambda^\varepsilon, \mu^\varepsilon > 0$ which by virtue of the unfolding are defined with respect to material points in Y_m^α. In Section 4 we use a constant tensor in Y_m^α, thus $\lambda^\varepsilon, \mu^\varepsilon$ are constants.

We shall record the homogenized mesoscopic problem reported in [6], see [7] for the proofs. It is expressed using homogenized material coefficients defined through the solutions of auxiliary microscopic problem known as the corrector basis functions. In the following text we present all microscopic problems constituting the mesoscopic homogenized medium.

3.3.2.   Microscopic problems and corrector basis functions

In what follows we shall use the following bilinear form:

$$a_y^d(\mathbf{w}, \mathbf{v}) = \fint_{Y_d} (\mathbf{D}\nabla_y^S\mathbf{w}) : \nabla_y^S\mathbf{v}, \tag{7}$$

where $\fint_{Y_d} = |Y|^{-1}\int_{Y_d}$ for $d = m, c$. We define the transformation vectors $\mathbf{\Pi}^{ij} = (\Pi_k^{ij})$, $i, j, k = 1, 2, 3$, whose components $\Pi_k^{ij} = y_j\delta_{ik}$ are constituted by coordinates y_j. In following text we denote the Sobolev space $[W^{1,2}(Y^\alpha)]^3$ of Y-periodic vector functions by $\mathbf{H}_\#^1(Y^\alpha)$.

We shall now define $\boldsymbol{\omega}^{ij}, \boldsymbol{\omega}^P$, the characteristic responses of the microstructure, which are solutions of the following microscopic problems: Find $\boldsymbol{\omega}^{ij} \in \mathbf{H}_\#^1(Y^\alpha)$ and $\boldsymbol{\omega}^P \in \mathbf{H}_\#^1(Y^\alpha)$ satisfying

$$a_y^m(\boldsymbol{\omega}^{ij} + \mathbf{\Pi}^{ij}, \mathbf{v}) = 0, \quad i, j = 1, \ldots, 3\,,$$

$$a_y^m(\boldsymbol{\omega}^P, \mathbf{v}) = \fint_{\Gamma_m} \mathbf{v} \cdot \mathbf{n}^m \mathrm{d}S_y. \tag{8}$$

---

[1]The convergence of the weak formulation can be found in the [6].

[2]δ_{ik} is the Kronecker symbol.

3.3.3. Homogenized coefficients

The material obtained by upscaling from the microscopic scale to the mesoscopic one is characterized by three effective coefficients, $\mathbb{A}^\alpha$, $\mathbf{B}^\alpha$ and M^α, which are expressed using the computed corrector functions $\boldsymbol{\omega}^{ij}$, $\boldsymbol{\omega}^P$ as follows:

$$
\begin{aligned}
A^\alpha_{ijkl} &= a^m_y(\boldsymbol{\omega}^{ij} + \boldsymbol{\Pi}^{ij}, \boldsymbol{\omega}^{kl} + \boldsymbol{\Pi}^{kl}), \\
B^\alpha_{ij} &= -\fint_{Y_m} \mathrm{div}_y \boldsymbol{\omega}^{ij}, \\
M^\alpha &= a^m_y(\boldsymbol{\omega}^P, \boldsymbol{\omega}^P).
\end{aligned}
\tag{9}
$$

The tensors $\mathbb{A}^\alpha$ and $\mathbf{B}^\alpha$ are symmetric, i.e. $\mathbb{A} = (A_{ijkl})$ satisfies $A^\alpha_{ijkl} = A^\alpha_{klij} = A^\alpha_{jikl}$ and $\mathbb{B}^\alpha = (B^\alpha_{ij})$ satisfies $B^\alpha_{ij} = B^\alpha_{ji}$. It can be shown, [6], that $M^\alpha > 0$. Further we may introduce

$$
\hat{\boldsymbol{B}}^\alpha = \boldsymbol{B}^\alpha + \phi \boldsymbol{I}, \qquad \hat{M}^\alpha = M^\alpha + \phi\gamma,
\tag{10}
$$

where $\hat{\mathbf{B}}^\alpha$ is the tensor of the Biot coefficients and $\hat{M}^\alpha$ is the effective Biot modulus of compressibility, which expresses the complete compressibility of the fluid and of the matrix deformed by the pore fluid pressure, [6]. The tensor $\mathbb{A}^\alpha$ is the effective elasticity tensor of the drained skeleton.

3.4. Mesoscopic problem

This section summarizes the upscaling procedure to obtain effective material properties relevant to the macroscopic scale. Thus, we shall introduce the poroelastic problem on the mesoscopic scale, using effective coefficients $\mathbb{A}^\alpha$, $\hat{\mathbf{B}}^\alpha$ and M^α obtained by upscaling the microstructure. This poroelastic model describes the behavior of the matrix part on the mesoscopic scale.

The domain Ω^β is decomposed as in (1)–(2) introduced for the heterogeneous microstructure, here representing the heterogeneous mesoscopic structure. We recall that the matrix $\Omega^{\beta,\varepsilon}_m$ is now formed by the porous medium associated with the upscaled microstructure of the α-level, and "canals". Canals $\Omega^{\beta,\varepsilon}_c$ are filled with the fluid and connected with pores of the α-level.

Since the α- and β-level porosities are mutually connected, the pressure $\bar{p}$ is evenly distributed through the fluid on both levels and can be characterized only by one scalar value only. The mesoscale matrix is loaded by the volume-force field $\hat{\boldsymbol{f}}^\alpha = (1 - \phi^\alpha)\boldsymbol{f}^\alpha$ and mean surface traction $\bar{\boldsymbol{g}}^\alpha := (1 - \phi^\alpha_s)\boldsymbol{g} + \phi^\alpha_s(-\bar{p})\boldsymbol{n}$ on $\partial_{ext}\Omega^{\beta,\varepsilon}_m$. The pores $\Omega^{\beta,\varepsilon}_c$ are drained out through $\partial_{ext}\Omega^{\beta,\varepsilon}_c$. The total outflow from Ω^β is denoted as $J^{\beta,\varepsilon}$ and it incorporates also the flux from α-level pores and from the β-level pores, [6]. The displacement $\boldsymbol{u}^{\beta,\varepsilon} \in \mathbf{H}^1(\Omega^{\beta,\varepsilon}_m)$ and the pressure $\bar{p}^\varepsilon \in \mathbf{H}^1(\Omega^{\beta,\varepsilon}_m)$ satisfy the equation

$$
\int_{\Omega^{\beta,\varepsilon}_m} (\mathbb{A}^\alpha \nabla^S \mathbf{u}^{\beta,\varepsilon} - \bar{p}^\varepsilon \hat{\mathbf{B}}^\alpha) : \nabla^S \mathbf{v} + \bar{p}^\varepsilon \int_{\Gamma^{\beta,\varepsilon}} \mathbf{v} \cdot \mathbf{n}^m \, \mathrm{d}S_x =
$$
$$
\int_{\partial_{ext}\Omega^{\beta,\varepsilon}_m} \bar{\mathbf{g}}^\alpha \cdot \mathbf{v} \, \mathrm{d}S_x + \int_{\Omega^{\beta,\varepsilon}_m} \hat{\mathbf{f}}^\alpha \cdot \mathbf{v}, \quad \forall \mathbf{v} \in V(\Omega^{\beta,\varepsilon}_m)
\tag{11}
$$

and the volume conservation

$$
\int_{\Omega^{\beta,\varepsilon}_m} (\hat{\mathbf{B}}^\alpha : \nabla^S \mathbf{u}^{\beta,\varepsilon} + \int_{\partial\Omega^{\beta,\varepsilon}_c} \tilde{\mathbf{u}}^{\beta,\varepsilon} \cdot \mathbf{n}^c \, \mathrm{d}S_x + \bar{p}^\varepsilon [(M^\alpha) + \gamma\bar{\phi}^\alpha |\Omega^{\beta,\varepsilon}_m| + \gamma|\Omega^{\beta,\varepsilon}_c|] = -J^{\beta,\varepsilon},
\tag{12}
$$

where $\tilde{\boldsymbol{u}}^{\beta,\varepsilon}$ is the displacement extension to canals $\Omega^{\beta,\varepsilon}_c$ and $\bar{\phi}^\alpha = |\Omega^\alpha|^{-1} \int_{\Omega^\alpha} \phi^\alpha$ is the mean porosity[3].

---

[3] However, in this work we consider constant porosity, thus, $\phi^\alpha = \bar{\phi}^\alpha$.

Analogically to previous section, the domain Ω^β is generated as periodic lattice using RPC Y^β. Note that like domain Ω^β, RPC Y^β has the decomposition analogical to Y^α, see Eq. (6). The upscaling procedure described in [6, 7] leads to the mesoscopic auxiliary problems for corrector basis functions of the β-level. These are employed to express the effective coefficients relevant to the macroscopic level of the osteon.

3.4.1. Mesoscopic problems and corrector basis functions

In what follows, we record the mesoscopic problems in Y^β for the corrector basis functions of displacement, $\boldsymbol{\omega}_\beta^{ij}$ and $\boldsymbol{\omega}_\beta^P$. Find $\boldsymbol{\omega}_\beta^{ij} \in \mathbf{H}_\#^1(Y_m^\beta)$ and $\boldsymbol{\omega}_\beta^P \in \mathbf{H}_\#^1(Y_m^\beta)$ satisfying

$$
\begin{aligned}
&\int_{Y_m^\beta} \left[\mathbb{A}^\alpha \nabla_y^S (\boldsymbol{\omega}_\beta^{ij} + \boldsymbol{\Pi}_\beta^{ij}) \right] : \nabla_y^S \mathbf{v} = 0 \qquad \forall \boldsymbol{v} \in \mathbf{H}_\#^1(Y_m^\beta), \\
&\int_{Y_m^\beta} \left[\mathbb{A}^\alpha \nabla_y^S \boldsymbol{\omega}_\beta^P \right] : \nabla_y^S \mathbf{v} = - \int_{Y_m^\beta} \hat{\mathbf{B}}^\alpha : \nabla_y^S \mathbf{v} + \int_{\Gamma_Y^\beta} \mathbf{v} \cdot \mathbf{n}^m \, \mathrm{d}S_y \qquad \forall \boldsymbol{v} \in \mathbf{H}_\#^1(Y_m^\beta),
\end{aligned}
\tag{13}
$$

where transformation vector $\boldsymbol{\Pi}_\beta^{ij} = (\Pi_{k,\beta}^{ij})$, $i, j, k = 1, 2, 3$ have components $\Pi_{k,\beta}^{ij} = y_j^\beta \delta_{ik}$ are constituted by coordinates y_j^β of RPC Y^β.

While the solutions $\boldsymbol{\omega}_\beta^{ij}$ express fluctuations with respect to the local macroscopic unite strain, the $\boldsymbol{\omega}_\beta^P$ expresses the local response with respect to the unit pore pressure, [6].

3.4.2. Homogenized coefficients

The corrector functions specified in the previous section are involved in the expressions of the effective material coefficients relevant to the macroscopic body with porosities on micro- and mesoscale and are denoted by $\mathbb{A}, \boldsymbol{B}, M$ (on the macroscale the superscript β is not necessary and has been released). These expressions are as follows

$$
A_{ijkl} = \fint_{Y_m^\beta} \left[\mathbb{A}^\alpha \nabla_y^S (\boldsymbol{\omega}_\beta^{kl} + \boldsymbol{\Pi}_\beta^{kl}) \right] : \nabla_y^S \mathbf{v}(\boldsymbol{\omega}_\beta^{ij} + \boldsymbol{\Pi}_\beta^{ij}),
\tag{14}
$$

$$
B_{ij} = \fint_{Y_m^\beta} \hat{\mathbf{B}}^\alpha : \nabla_y^S \mathbf{v}(\boldsymbol{\omega}_\beta^{ij} + \boldsymbol{\Pi}_\beta^{ij}) - \fint_{Y_m^\beta} \mathrm{div}_y \boldsymbol{\omega}_\beta^{ij},
\tag{15}
$$

$$
M = \fint_{Y_m^\beta} \left[\mathbb{A}^\alpha \nabla_y^S (\boldsymbol{\omega}_\beta^p) \right] : \nabla_y^S \mathbf{v}(\boldsymbol{\omega}_\beta^p).
\tag{16}
$$

Further, we introduce

$$
\hat{\mathbf{B}} := \mathbf{B} + \phi^\beta \mathbf{I}, \qquad \hat{M} := M + \gamma \bar{\phi}^\beta + (M^\alpha + \gamma \bar{\phi}^\alpha)(1 - \bar{\phi}^\beta) .
\tag{17}
$$

These effective coefficients are analogical to the classical Biot model coefficients. Advantageously, the given formulae enable to compute them for a given representative cells at both the micro- and mesoscopic levels.

3.4.3. Macroscopic problem

In the previous section, we derive the equations for effective coefficients relevant to the macroscopic poroelastic body with porosities distributed at the two scales. Responses of such a body

are described by the displacement $\mathbf{u}$ and by the pressure $\bar{p}$ satisfying

$$\int_{\Omega^\beta} (\mathbb{A}\nabla_x^S \mathbf{u} - \bar{p}\hat{\mathbf{B}}) : \nabla_x^S \mathbf{v} = \int_{\Omega^\beta} (1 - \phi^\beta)\mathbf{f}^\alpha \cdot \mathbf{v} + \int_{\partial\Omega^\beta} \bar{\mathbf{g}}^\beta \cdot \mathbf{v}\, \mathrm{d}S_x \quad \forall \boldsymbol{v} \in \mathbf{H}^1(\Omega^\beta),$$

$$\int_{\Omega^\beta} \hat{\mathbf{B}}\nabla_x^S \mathbf{u} + \bar{p}\hat{M}|\Omega^\beta| = -J^\beta \qquad \forall \boldsymbol{v} \in \mathbf{H}^1(\Omega^\beta), \tag{18}$$

where in analogy with $\bar{\boldsymbol{g}}^\beta$ introduced above at the mesoscopic scale,

$$\bar{\boldsymbol{g}}^\beta := (1 - \phi_S^\beta)\bar{\boldsymbol{g}}^\alpha + \phi_S^\beta(-\bar{p})\mathbf{n} \tag{19}$$

is the mean surface stress and $\bar{\phi}_S^\beta$ is the mean surface β-level porosity.

   Now we have a complete set of equations for obtaining the poroelastic properties of one single osteon in cortical bone tissue. The effective coefficients can be used for further applications and can be also associated with the Biot poroelasticity model, from which the increase of fluid content J^β can be computed.

   In the section below, we assume that the interface on both levels $\Gamma^{\alpha,\varepsilon}$ and $\Gamma^{\beta,\varepsilon}$ is impermeable, but porosities on α- and β- beta level are mutually connected; this configuration results in one hydrostatic pressure $\bar{p}$ in all porosity levels, see section 3.4.3. In addition, the matrix cannot be drained throught $\partial_{ext}\Omega_m^{\beta,\varepsilon}$, thus $\phi_S^\beta = 0$ on the exterior surface. In this case $\bar{\boldsymbol{g}}^\beta(\bar{p}) = \bar{\boldsymbol{g}}^\beta$ is independent of the pore pressure and also external flux $J^\beta = 0$.

4. Two-level computational homogenization

In this section we provide illustrations to the two-level computational homogenization. We consider an idealized structure of the cortical bone tissue characterized at the micro- and mesoscopic scales using the representative periodic cells Y^α and Y^β, respectively; the details will be given in Section 4.1. We use the finite element method (FEM) to discretize in space the weak formulations presented in previous sections. As explained above, the linearity of the multiscale problem leads to a computational algorithm consisting of the following steps:

1. Solve the auxiliary corrector problems in the RPC Y^α defined by Eq. (8) to obtain the local response functions $\omega^{ij}\big|^\alpha, \omega^p\big|^\alpha$.

2. Using $\omega^{ij}\big|^\alpha, \omega^p\big|^\alpha$ substituted in formulae (9) and (10), compute effective coefficients $\mathbb{A}^\alpha$, $\hat{\mathbf{B}}^\alpha$ and $\hat{M}^\alpha$ which characterize the matrix phase of the β-level structure.

3. Solve the auxiliary corrector problems in the RPC Y^β given by Eq. (13) to obtain local response functions $\omega^{ij}\big|^\beta, \omega^p\big|^\beta$.

4. Using $\omega^{ij}\big|^\beta, \omega^p\big|^\beta$ substituted in formulae (15) and (17), compute effective coefficients $\mathbb{A}^\beta$, $\hat{\mathbf{B}}^\beta$ and $\hat{M}^\beta$ involved in the macroscopic model.

5. Using the effective coefficients $\mathbb{A}^\beta$, $\hat{\mathbf{B}}^\beta$ and $\hat{M}^\beta$, solve the macroscopic problem (18) imposed in domain Ω.

   Although the Neumann boundary conditions are assumed in Eq. (18), other boundary conditions can be prescribed. The classical formulation yields the equilibrium condition

$$-\nabla \cdot (\mathbb{A}\nabla_x^S \mathbf{u} - \bar{p}\hat{\mathbf{B}}) = (1 - \phi^\beta)\mathbf{f}^\alpha \quad \text{in } \Omega\,, \tag{20}$$

which is accompanied by the mass balance (18)$_2$. In general, the boundary conditions may involve the Dirichlet type boundary conditions imposed on $\partial_u\Omega \subset \partial\Omega$, whereas the traction (Neumann) conditions are prescribed on the rest of the boundary, $\partial_\sigma\Omega \subset \partial\Omega \subset \partial_u\Omega$, thus,

$$\boldsymbol{n} \cdot (\mathbb{A}\nabla_x^S\mathbf{u} - \bar{p}\hat{\mathbf{B}}) = \bar{\mathbf{g}}^\beta \qquad \text{on } \partial_\sigma\Omega \,, \tag{21}$$

where $\boldsymbol{n}$ is the unit normal vector on $\partial_\sigma\Omega$. Recalling definition (19) of $\bar{\boldsymbol{g}}^\beta$, it should be noted, that (21) involves $\bar{p}$ through $\bar{\boldsymbol{g}}^\beta$ and $\bar{\boldsymbol{g}}^\alpha$ if the surface porosities ϕ_S^β and ϕ_S^α do not vanish. For discussion of possible cases of the boundary conditions and their consequences on the symmetry of problem (18) we refer to [7].

4.1. Geometrical representation

As discussed in the introduction, the cortical bone tissue can be represented by the hierarchical porous structure which is defined at the two levels by the RPCs Y^α and Y^β, see Fig. 2. The two-level upscaling procedure yields the effective material properties of bone osteon which constitutes the macroscopic body. All dimensional parameters describing employed geometrical features[4] are listed in Table 2. In this study we consider an artificial, simplified geometry of the canalicular and lacunar porosities which can easily be parameterized. This allows us to describe qualitatively influences of the selected structural features on the effective material properties of the upscaled bone.

(a)   (b)   (c)
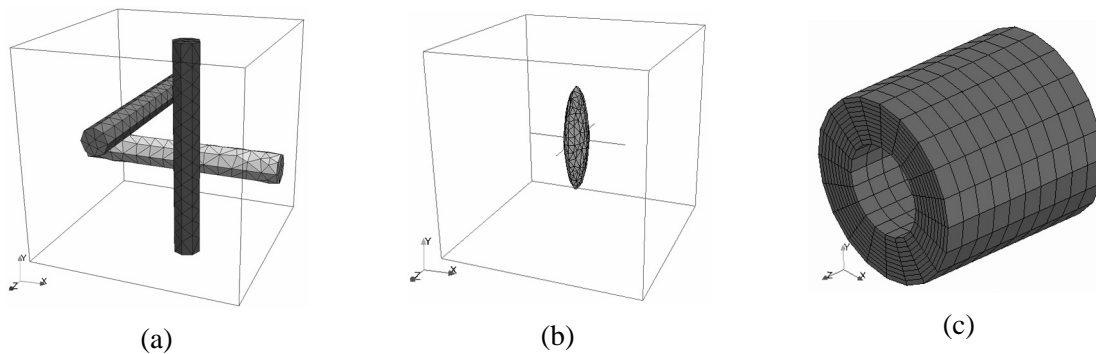
Fig. 2. Geometry representations of (a) RPC Y^α, (b) RPC Y^β and (c) macroscopic level body

Table 2. Parameters of geometrical configuration

Symbol	Parameter	Unit	Value
L_α	characteristic length of RPC on micro-level	μm	4.3
L_β	characteristic length of RPC on meso-level	μm	43.0
$r_x = d_x/2$	radius of canaliculi in x-direction	μm	0.6
$r_y = d_y/2$	radius of canaliculi in y-direction	μm	0.6
$r_z = d_z/2$	radius of canaliculi in z-direction	μm	0.6
a_0	semi-axis of ellipsoid in x-direction	μm	2.5
b_0	semi-axis of ellipsoid in y-direction	μm	12.5
c_0	semi-axis of ellipsoid in z-direction	μm	5.0

---

[4]In this section we use labelling of coordinate axes by x, y, z rather than $1, 2, 3$.
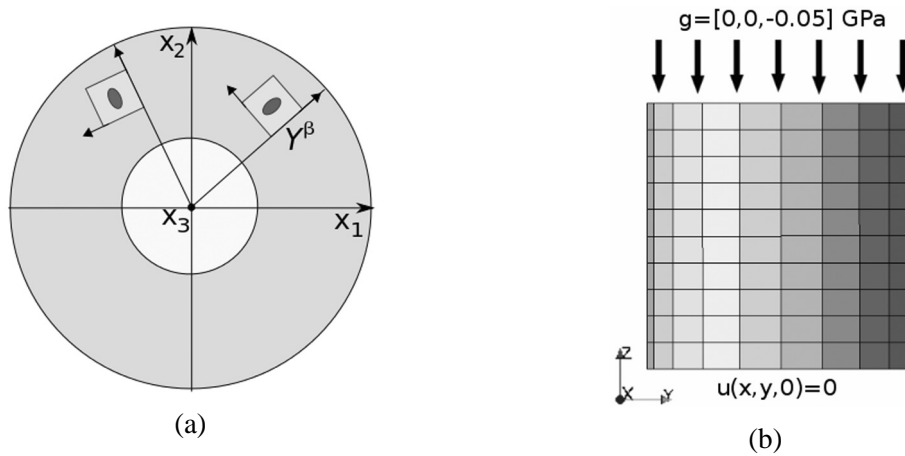
Fig. 3. (a) Circumferential orientation of RPC Y^β in cylindrical macroscopic body, (b) Loading and boundary conditions of macroscopic body

At the microscopic level, the bone matrix is represented by the cubic RPC Y^α of the edge size L_α. The solid phase corresponding to the bone matrix occupies domain Y_m^α. The canalicular pores (domain Y_c^α) are represented by three cylindrical channels defined by radii r_x, r_y and r_z. We choose them in such a way that the cross-section area of each channel is approximately equal to the total cross-section area of all actual canaliculi which lead in the corresponding direction. Although geometrically disconnected, in a "physical sense" we adhere the assumption of their mutual cennectness.

At the mesoscopic level, the lacunar porosity is represented by RPC Y^β of the edge size L_β. The porous matrix occupying domain Y_m^β is constituted by the upscaled canalicular porosity, so that it represents a network of orthogonal channels leading in x-, y- and z-directions. A single ellipsoidal inclusion occupies domain Y_c^β, which represents one lacunae, is defined by three semi-axes a_0, b_0, c_0. Recall that both the α and β porosities form one connected porosity associated with one pressure $\bar{p}$.

In the present study, the macroscopic level is represented by a single bone osteon occupying domain Ω, although at this level the bone tissue can also be described approximatively as a heterogeneous structure constituted by periodically distributed osteons, as considerd, e.g., in [5]. Thus, Ω is shaped as a hollow cylinder, see Fig. 2c. The material model obtained using the two-level homogenization can be associated with a local coordinate system, in general. Below we consider that the material structure is locally periodic, generated by cell Y^β which is aligned with the radial, tangential and axial macroscopic coordinate axes related naturally to the cylindrical geometry, see Fig. 3a. Obviously, the orientation of the α-level anisotropy is fixed within the mesoscopic RPC Y^β.

4.2. Numerical examples

The purpose of this example is to show how different structures at micro- and mesoscopic level influence the homogenized coefficients and the macroscopic response. For better understanding of how each level influence the final effective coefficients, we present following three numerical examples.

Example 1 We modify the canalicular porosity ϕ^α by changing the diameter of one of the three cylindrical channels aligned with the x-axis. The geometry representing RPC Y^β is preserved, see Fig. 4a.
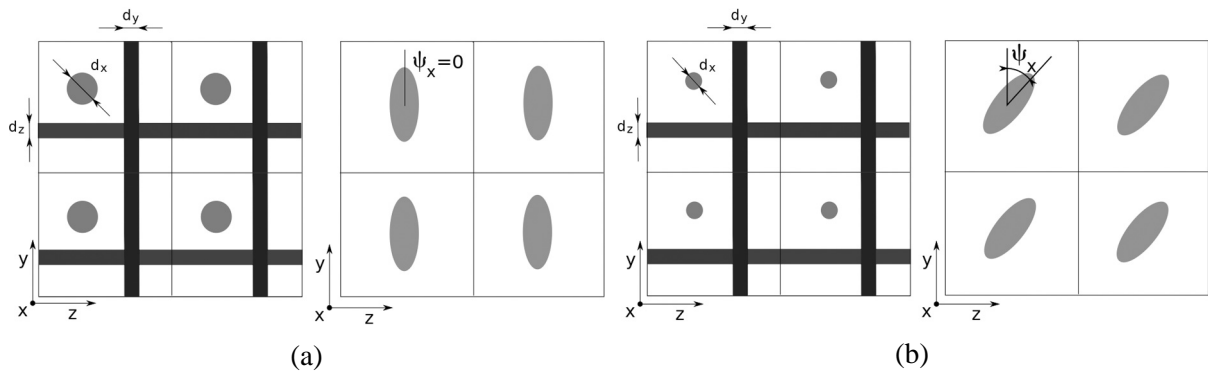
208

Fig. 4. Numerical example schemes: (a) Example 1 – changing diameter d_x on the RPCs Y^α geometry while preserving lacunae position in RPC Y^β; (b) Example 2 – while preserving RPC Y^α ($d_x = d_y = d_z$), rotating ellipsoid conclusion in RPC Y^β on axes x, y and z (rotation angle $\psi_i \in \langle 0, \pi/2 \rangle, i = x, y, z$)

Example 2 While preserving the geometry representation of RPC Y^α, we change orientation of ellipsoidal inclusion in RPC Y^β by rotating it subsequently on one of its axes by angles ψ_i, $i = x, y, z$, see Fig. 4b.

Example 3 We solve the macroscopic problems with effective material coefficients obtained according to Example 1 and Example 2, as described above.

In the following text, we report numerical results obtained for these three numerical examples. First, we compute final effective coefficients for models Example 1 and Example 2 and then use them to solve the macroscopic problems, as specified in Example 3. The two-scale, two-level homogenization was implemented in our in-house developed FEM software *SfePy*, for more information see the website *sfepy.org*.

4.3. Effective coefficients

We use an isotropic material with Young's modulus $E = 18\,\text{GPa}$ and Poisson's ratio $\nu = 0.3$ to describe the solid matrix representing bone tissue in RPC Y^α, while the fluid is characterized by its compressibility $\gamma = 0.9$. These values were choosen as our estimation of the cortical bone material properties relevant to the microstructure (the canalicular porosity level) on the basis of information found in the literature [11], see also [9].

The resulting homogenized material is orthotropic, whereby the effective compliance tensor $\mathbb{A}^{-1}$ is symetric, attaining the following form

$$
\mathbb{A}^{-1} = \begin{bmatrix}
\frac{1}{E_1} & -\frac{\nu_{21}}{E_2} & -\frac{\nu_{31}}{E_3} & 0 & 0 & 0 \\
-\frac{\nu_{12}}{E_1} & \frac{1}{E_2} & -\frac{\nu_{32}}{E_3} & 0 & 0 & 0 \\
-\frac{\nu_{13}}{E_1} & -\frac{\nu_{23}}{E_2} & \frac{1}{E_3} & 0 & 0 & 0 \\
0 & 0 & 0 & \frac{1}{G_{12}} & 0 & 0 \\
0 & 0 & 0 & 0 & \frac{1}{G_{23}} & 0 \\
0 & 0 & 0 & 0 & 0 & \frac{1}{G_{31}}
\end{bmatrix}, \tag{22}
$$

where E_1, E_2, E_3 are Young's moduli in directions 1, 2, 3. ν_{ij} represents the Poisson's ratio for the strain in direction j while loaded in direction i. G_{12}, G_{23}, G_{31} are shear moduli in 1-2, 2-3 a 3-1. Due to symmetry $\frac{\nu_{ij}}{E_i} = \frac{\nu_{ji}}{E_j}$, the orthotropic material can be described by only 12 material constants stated above.

4.3.1. Example 1

First, let us give an example of effective coefficients resulting from upscaling to the macroscopic level. The coefficients

$$
\mathbb{A}^{\beta} =
\begin{bmatrix}
1.801 \cdot 10^1 & 7.064 \cdot 10^0 & 6.731 \cdot 10^0 & 1.501 \cdot 10^{-4} & -1.404 \cdot 10^{-4} & -1.851 \cdot 10^{-4} \\
7.064 \cdot 10^0 & 1.804 \cdot 10^1 & 6.730 \cdot 10^0 & 1.446 \cdot 10^{-4} & -1.798 \cdot 10^{-4} & 8.559 \cdot 10^{-6} \\
6.731 \cdot 10^0 & 6.730 \cdot 10^0 & 1.806 \cdot 10^1 & 2.876 \cdot 10^{-6} & -5.283 \cdot 10^{-4} & 5.491 \cdot 10^{-6} \\
1.501 \cdot 10^{-4} & 1.445 \cdot 10^{-4} & 2.723 \cdot 10^{-6} & 5.549 \cdot 10^0 & 2.040 \cdot 10^{-6} & -7.826 \cdot 10^{-5} \\
-1.408 \cdot 10^{-4} & -2.031 \cdot 10^{-4} & -5.507 \cdot 10^{-4} & 2.308 \cdot 10^{-6} & 5.205 \cdot 10^0 & 1.637 \cdot 10^{-4} \\
-1.852 \cdot 10^{-4} & 7.385 \cdot 10^{-6} & 4.367 \cdot 10^{-6} & -7.824 \cdot 10^{-5} & 1.648 \cdot 10^{-4} & 5.205 \cdot 10^0
\end{bmatrix},
$$

$$
\hat{\mathbf{B}}^{\beta} = \begin{bmatrix} 1.096 \cdot 10^0, & 1.096 \cdot 10^0, & 1.097 \cdot 10^0, & -1.134 \cdot 10^{-5}, & -3.161 \cdot 10^{-6}, & -3.177 \cdot 10^{-7} \end{bmatrix},
$$

$$
\hat{M}^{\beta} = 1.004 \cdot 10^{-4}
$$

were computed for the start configuration, i.e., $r_x = r_y = r_z = 0.6\,\mu$m and $\psi_x = \psi_y = \psi_z = 0$. When commponents smaller than 10^{-3} are neglected, stiffness $\mathbb{A}^{\beta}$ attain the form such of orthotropic material.

A shown in Fig. 5a, the macroscopic effective coefficients vary with the total porosity $\phi_{\gamma} = \phi_{\alpha} + \phi_{\beta} - \phi_{\alpha}\phi_{\beta}$ since porosity ϕ_{α} is being changed. For better understanding how variation of porosity on α-level influence the characteristics of macroscopic body, we transformed effective stiffness tensor into components of Young's modulus E_i, Poisson's ratio ν_{ij}, $i,j = 1, 2, 3, i \neq j$
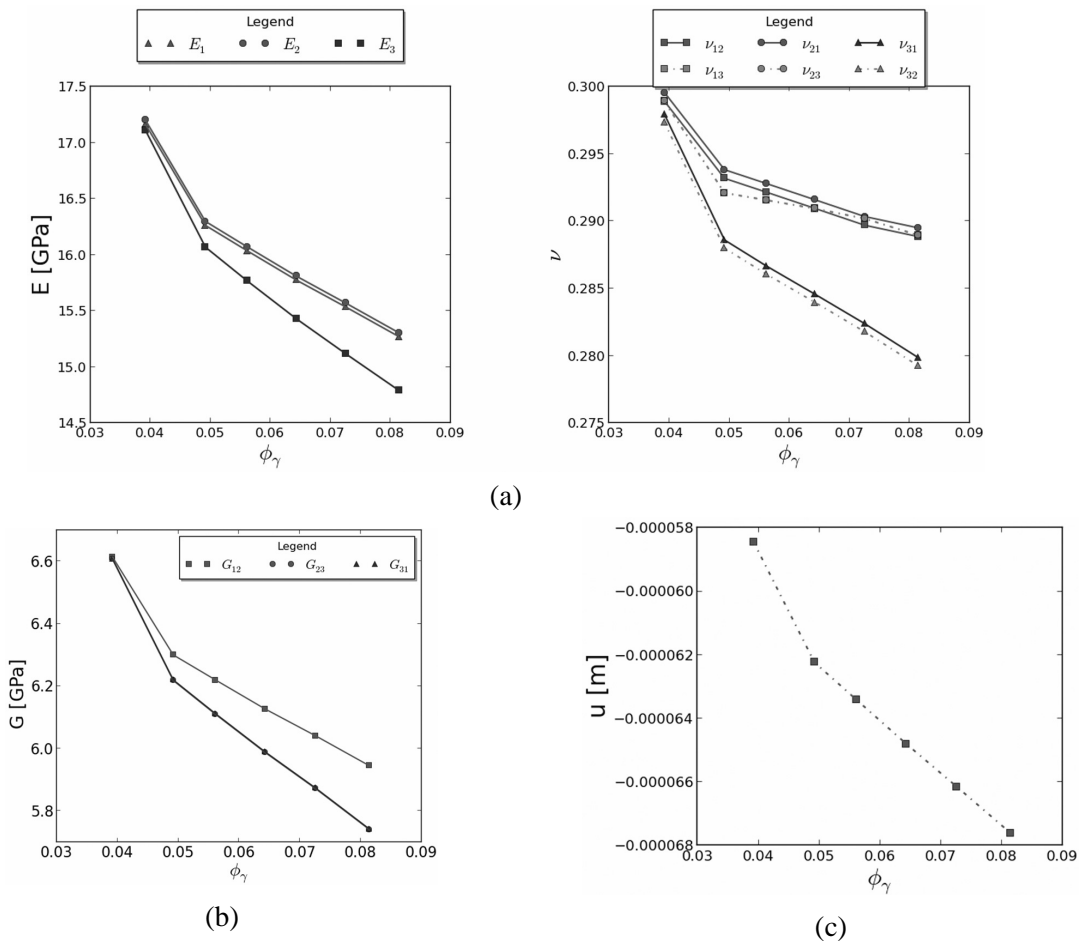

Fig. 5. Example 1 – Effective coefficients influenced by varying x-direction canaliculi radius r_x

and shear modulus G_{12}, G_{23}, G_{31}. It is clear, that as porosity rises, the solid phase is being replaced by the fluid part in the RPC Y^α, thus the curves of components of elastic coefficients decrease.

4.3.2. Example 2

A more complex influence of the orientation of the lacunae on the elastic coefficients is apparent in Figs. 6a, 6b and 6c, where we display the dependence of Young's modulus and Poisson's ratio on rotation angle ψ_i, $i = x, y, z$. The Dependence of sheare modulus G on ψ_i is then shown in Figs. 7a, 7c and 7e. In this study, the varying mutual positions of the ellipsoidal inclusions of the neighbouring cells (copies of Y^β), have to be taken into account. As the ellipsoids rotate, the cross-sectional areas of the solid phase in the planes perpendicular to main axes vary, which results into components of effective elastic coefficients having different trends.

4.4. Macroscopic problem solution

Using effective coefficients obtained above for various volume fractions, or varying orientations of the lacunae at the mesoscopic level, we now solve the macroscopic problem given by Eq. (18). In order to enable that to the two parameteric studies considered in the Example 1 and Example 2 can be compared, we use for both the same geometry representation of macroscopic body (see Fig. 2c) and the same boundary conditions. The single bone osteon is loaded by a uniform traction force $g = [0, 0, -5]$ MPa on the upper face $z = l$, where l is the cylinder length aligned with the z-coordinate, and stuck to the rigid frame on the bottom face $z = 0$, see Fig. 3b. Note, that the RPC Y^β representing mesoscopic level structure are circumferentially arranged in the macroscopic body, see Fig. 3a, so that the ellipsoid orientation with respect to the local tangential and radial axes is fixed.

Responses to the static loading of the macroscopic body for materials studied in Example 1 are shown in Fig. 5c. We display only the z-component of displacement, u_z, because in this direction maximal displacements appear. As expected, we may see that the curve of u_z follows the trend of E_3. Similarily, curves of u_z displacement for materials studied in Example 2 follow the effective elastic coefficients, see Figs. 7b, 7d and 7f.

5. Conclusion

In this paper we presented the three-scale model of cortical bone tissue obtained by homogenization procedure based on [6]. Such model was motivated by a strictly hierarchical structure of a cortical bone saturated by a bone fluid. We briefly described the computational steps leading to evaluation of the effective coefficients on the micro- and mesoscopic scale levels, the latter being involved in the macroscopic problem formulation. The resulting homogenized model describes deformation of the fluid saturated double-porous body in response to a static loading by external forces and to an injection of slightly compressible fluid.

The solutions of this model was implemented in the software *SfePy* and two numerical examples were presented, showing the influence of selected micro- and mesostructure geometrical features on the effective material poroelastic properties apparent at the macroscopic scale. As an advantage, this two-scale hierarchical approach allows for geometrically based identification of the Biot material model. Therefore, this model can be used as a basis for further research not only in bone tissue mechanics, but also in tissue biomechanics in general, as well as in other fields of engineering sciences related to porous media.
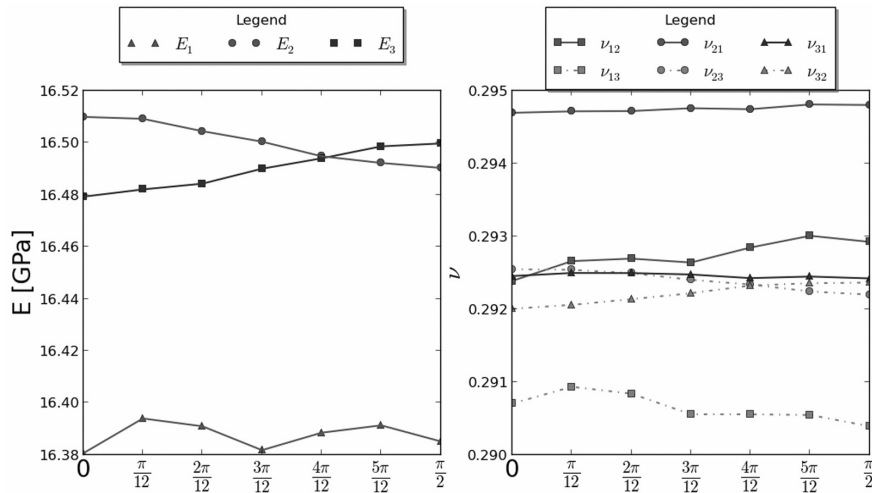
(a) Dependence of Young's modulus and Poisson's ratio on rotation angle ψ_x
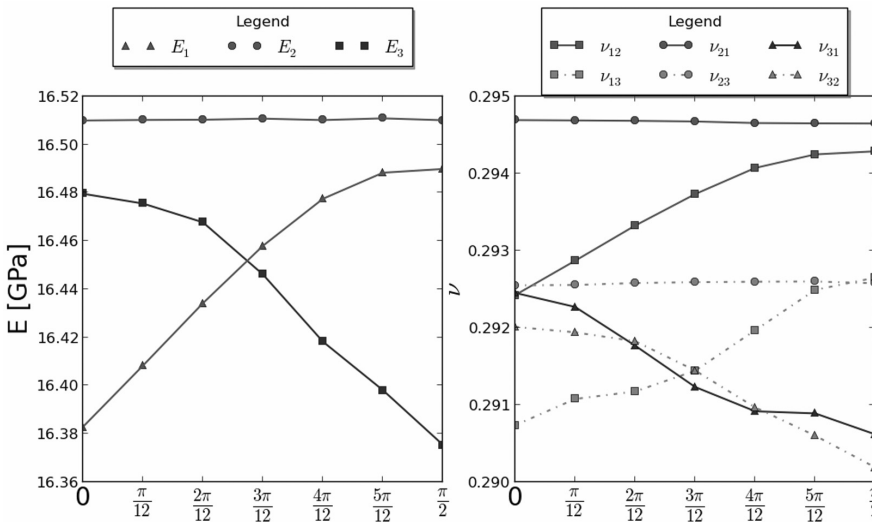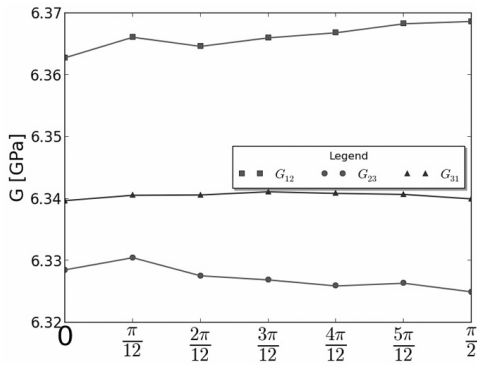

(b) Dependence of Young's modulus and Poisson's ratio on rotation angle ψ_y
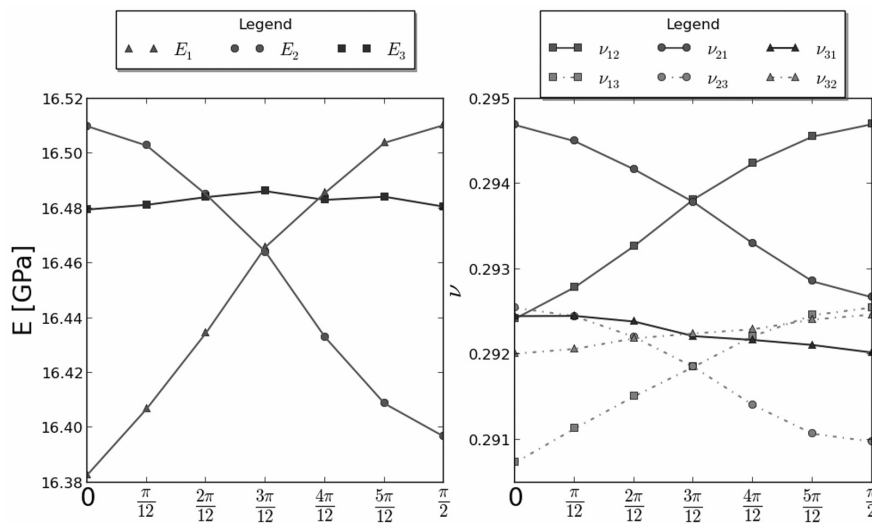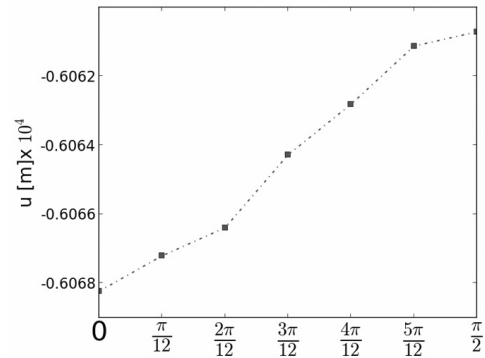

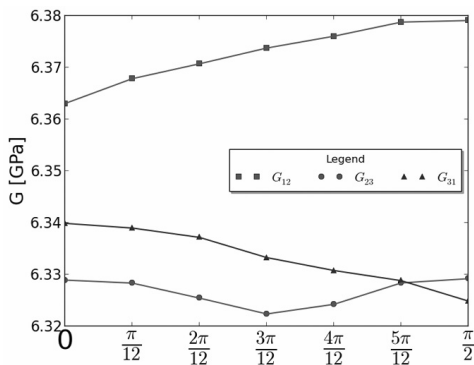(c) Dependence of Young's modulus and Poisson's ratio on rotation angle ψ_z

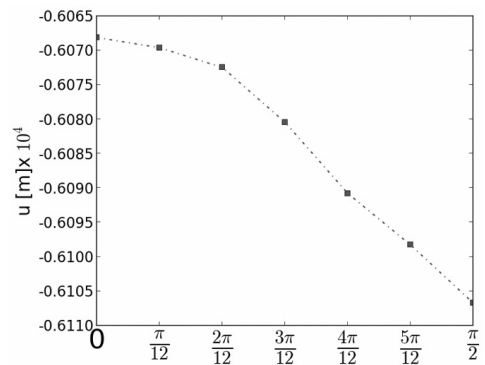Fig. 6. Example 2 – Effective coefficients influenced by rotation angle ψ_i of lacuna
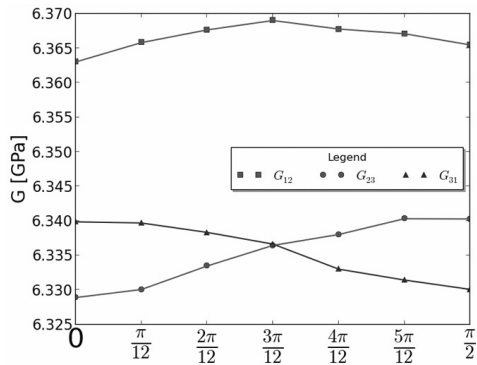
(a) Dependence of shear modulus G on ψ_x
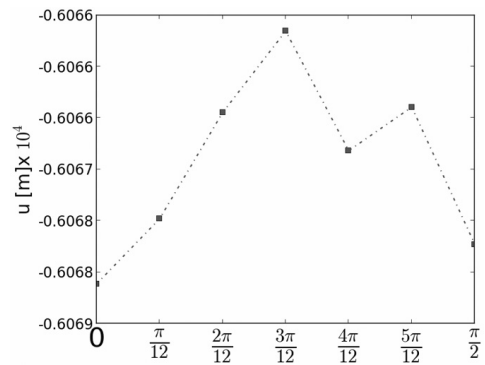
(b) Dependence of displacement u_z on ψ_x

(c) Dependence of shear modulus G on ψ_y

(d) Dependence of displacement u_z on ψ_y

(e) Dependence of shear modulus G on ψ_z

(f) Dependence of displacement u_z on ψ_z

Fig. 7. Example 2 – (Left) Components of shear moduli influenced by rotation angle ψ_i of lacuna; (Right) z-component of displacement u_z influenced by rotation angle ψ_i of lacuna

Acknowledgements

References

[1] Barenblatt, G. I., Zheltov, Iu P., Kochina, I. N., Basic concepts in the theory of seepage of homogeneous liquids in fissured rocks, Journal of Applied Mathematics and Mechanics 24 (5) (1960) 1 286–1 303.

[2] Beno, T., Yoon, Y.-J., Cowin, S. C., et al., Estimation of bone permeability using accurate microstructural measurements, Journal of Biomechanics 39 (13) (2006) 2 378–2 387.

[3] Mikelic, A., Wheeler, M., On the interface law between a deformable porous medium containing a viscous fluid and an elastic body, Mathematical Models and Methods in Applied Sciences 22 (2012) 1–32.

[4] Rho, J. Y., Kuhn-Spearing, L., Zioupos, P., Mechanical properties and the hierarchical structure of bone, Medical Engineering & Physics 20 (2) (1998) 92–102.

[5] Rohan, E., Naili, S., Cimrman, R., Lemaire, T., Multiscale modeling of a fluid saturated medium with double porosity: Relevance to the compact bone, Journal of the Mechanics and Physics of Solids 60 (2012) 857–881.

[6] Rohan, E., Naili, S., Cimrman, R., Lemaire, T., Hierarchical homogenization of fluid saturated porous solid with multiple porosity scales, Comptes Rendus Mecanique 340 (10) (2012) 688–694.

[7] Rohan, E., Naili, S., Lemaire, T., Double porosity in fluid-saturated elastic media — deriving effective parameters by hierarchical homogenization, Continuum Mechanics and Thermodynamics (2014). (submitted)

[8] Rohan, E., Shaw, S., Whiteman, J. R., Poro-viscoelasticity modelling based on upscaling quasistatic fluid-saturated solids, Computational Geosciences 18 (2014) 883–895.

[9] Turjanicová, J., Electro-mechanical coupling in porous bone structure — homogenization method application, Master thesis, University of West Bohemia, Pilsen, 2013.

[10] Warren, J. E., Root, P. J., The behavior of naturally fractured reservoirs, Society of Petroleum Engineers Journal 3 (3) (1963) 245–255.

[11] Yoon, Y. J., Cowin, S. C., An estimate of anisotropic poroelastic constants of an osteon, Biomechanics and Modeling in Mechanobiology 7 (1) (2008) 13–26.